Supporting Information

Structure-guided engineering of membrane-binding regions for surfactant-free solubilization of direct electron transfer-type alcohol dehydrogenase

Konatsu Ichikawa[a], Taiki Adachi[*a], Tomoko Miyata[b,c], Fumiaki Makino[b,c,d], Keiichi Namba[b,c], Yuki Kitazumi[a], Osamu Shirai[a], and Keisei Sowa[*a]

[a] *Division of Applied Life Sciences, Graduate School of Agriculture, Kyoto University, Sakyo, Kyoto 606-8502, Japan*

[b] *Graduate School of Frontier Biosciences, The University of Osaka, Suita, Osaka 565-0871, Japan*

[c] *JEOL YOKOGUSHI Research Alliance Laboratories, The University of Osaka, Suita, Osaka 565-0871, Japan*

[d] *JEOL Ltd., Akishima, Tokyo 196-8558, Japan*

*Corresponding authors:

Dr. Taiki Adachi, E-mail address: adachi.taiki.5z@kyoto-u.ac.jp

Dr. Keisei Sowa, E-mail address: sowa.keisei.2u@kyoto-u.ac.jp

Experimental

Materials and Chemicals

Multi-walled carbon nanotubes functionalized with the carboxylic group (CNT-COOH, outer diameter: 15 ± 5 nm, length: 1–5 μm) were purchased from NanoLab Inc. (USA). Protein markers and 12.5% acrylamide gels for sodium dodecyl sulfate polyacrylamide gel electrophoresis (SDS-PAGE) were obtained from Nacalai Tesque Inc. (Japan) and Atto Co. (Japan), respectively. A P′ medium was prepared with 1% yeast extract (Oriental Yeast Co., Ltd., Japan), 1% hipolypeptone (Shiotani M.S. Co., Ltd., Japan), 0.5% glucose, and 2% glycerol. All other chemicals were obtained from Wako Pure Chemical Industries Ltd. (Japan), unless otherwise stated. All aqueous solutions were prepared using ultrapure water. The bacterial strains and plasmids used in this study are summarized in Table S1. The *Gluconobacter oxydans* NBRC12528 Δ*adhAB*Δ*aldFGH* strain [1] was used as an expression host. Plasmids for expression were outsourced to VectorBuilder Japan Inc. (Japan).

Preparation of Crude Enzyme Solutions

The strains expressing wild-type recombinant alcohol dehydrogenase (rADH), Δ1, Δ2, Δ3, Δ1Δ2, Δ1Δ3, Δ2Δ3, and Δ1Δ2Δ3 variants were cultivated in a P′ medium, respectively. The grown cells were collected by centrifugation at 12,000 × *g* for 5 min at 4 °C, washed with 20 mM phosphate buffer (pH 6.0) twice, and resuspended in 20 mM phosphate buffer (pH 6.0) containing 2 mM $CaCl_2$ and 10% sucrose. The resuspended cells were disrupted twice using a French Press G-M (Glen Milles Inc., USA) at 1,000 psi. Cell debris was removed from the suspension by centrifugation at 12,000 × *g* for 5 min. The supernatant was centrifuged at 200,000 × *g* for 1 h at 4 °C. The supernatant was collected as the soluble fraction. The precipitate was resuspended in 20 mM phosphate buffer (pH 6.0) containing 2 mM $CaCl_2$, 10% sucrose, and 1% Triton X-100, using a glass homogenizer. The suspension was stirred for 2 h at 4 °C to solubilize membrane proteins, and subsequently centrifuged at 200,000 × *g* for 1 h at 4 °C. The supernatant was collected as the membrane fraction.

Purification of rADH and sADH

rADH was purified according to the procedure in the literature [2]. sADH was purified as follows: pBBR1MCS-4-Padh-Δ1Δ2Δ3 variant was cultivated in a P′ medium to overexpress sADH. The cells were collected by centrifugation at 10,000 × *g* for 5 min at 4 °C, resuspended in 20 mM phosphate buffer (pH 6.0) containing 50 mM ethanol, $CaCl_2$, and 10% sucrose, and disrupted twice using the French Press G-M at 1000 psi. Cell debris was removed from the suspension by centrifugation at 12,000 × *g* for 5 min. The supernatant was centrifuged at 200,000 × *g* for 1 h at 4 °C. The supernatant was collected as the crude enzyme solution and loaded onto a TOYOPEARL DEAE-650M column (approximately 20 mL; Tosoh Bioscience, Japan) equilibrated with 20 mM phosphate buffer (pH 6.0) containing 5 mM ethanol, 2 mM $CaCl_2$, and 10% sucrose. The column was then washed with a 5-bed volume of the same buffer. The collected DEAE-passing fraction was loaded onto a CHT ceramic hydroxyapatite column (approximately 20 mL, Bio-Rad, USA) equilibrated with the same buffer. The column was then washed with a 5-bed volume of the same buffer. A linear gradient elution with phosphate buffer (pH 6.0) from 20–500 mM containing 5 mM ethanol, 2 mM $CaCl_2$, and 10% sucrose was conducted, and fractions with ethanol oxidation activity were collected. The collected fractions were concentrated to approximately 1 mL using 50 kDa ultrafiltration membranes and loaded onto Superdex 200 Increase 10/300 GL (Cytiva, Sweden) equilibrated with 150 mM phosphate buffer (pH 6.0) containing 2 mM $CaCl_2$ and 10% sucrose. The column was washed with a 5-bed volume of the same buffer, and fractions with ethanol oxidation activity were collected. The fractions were then combined and frozen in liquid nitrogen.

Enzyme Assay

The concentrations of the proteins were estimated using a Pierce bicinchoninic acid (BCA) protein assay kit (Thermo Fisher Scientific Inc., USA) with bovine serum albumin as the standard sample. SDS-PAGE was performed to determine the purity of the enzyme solutions. Spectrophotometric analysis of the ethanol-oxidizing/ferricyanide-reducing activity of the enzymes was performed at 25 °C and pH 5.5 by using a ferric-dupanol reagent [3]. One unit is defined as the amount of the enzyme that reacts with 1 μmol of ethanol (or 2 μmol ferricyanide) per minute.

Electrode Preparation

Glassy carbon electrodes (GCEs; 3 mm in diameter, BAS Inc., Japan) were polished successively with a 1.0 and 0.05 μm alumina slurry, sonicated in, and subsequently washed with distilled water. A 0.1 wt % CNT-COOH dispersion was prepared via sonication in distilled water for 2 h. A 10 μL aliquot of the CNT-COOH dispersion was applied onto the GCEs and dried at 70 °C. These electrodes are referred to as CNT-COOH/GCEs. A 10 μL aliquot of the enzyme solution (10 mg mL^{-1}) dissolved in 100 mM phosphate buffer (pH 6.0) containing 2 mM $CaCl_2$ was applied onto the surface of the electrodes. The electrodes were placed in a water-saturated atmosphere for 2 h at 4 °C. These working electrodes were referred to as rADH/CNT-COOH/GCE and sADH/CNT-COOH/GCE. The current density was calculated using the projective surface area (0.07 cm^2).

Electrochemical Measurements

Electrochemical measurements were conducted using an electrochemical analyzer (ALS650E, BAS Inc., Japan) and a rotating disk electrode instrument (RRDE-3A, BAS Inc., Japan). A platinum wire and homemade Ag|AgCl|sat. KCl electrodes were used as counter and reference electrodes, respectively. All potentials in this study were recorded against the reference electrode. All electrochemical measurements were performed in 100 mM acetate buffer (pH 5.5) under Ar-saturated conditions at 25 °C at a rotation speed (ω) of 4,000 rpm.

Cryo-EM Analysis of sADH

Data Collection

A 2.5 μL aliquot of the sADH solution (3 mg mL^{-1}) without sucrose containing 0.9% *n*-octyl-*β*-D-glucoside (OG) in consideration of the preferred orientation challenge was applied to a Quantifoil holey carbon support film grid (Cu R1.2/1.3), which was then frozen in liquid ethane using a FEI Vitrobot Mark IV (Thermo Fisher Scientific, USA) at 4 °C and 100% humidity [4]. The blotting and drain times were set to 3 and 2 s, respectively. Sample data was collected using a CRYO ARM 300 (JEOL, Japan) system equipped with a K3

direct electron detector camera (Gatan, USA), Ω-type energy filter with a 20 eV slit width, and cold field-emission electron gun operating at 300 kV. Images were recorded using serial-EM [5], and holes were detected using YoneoLocr [6]. Movie frames were recorded using a K3 camera at a calibrated magnification of 60,000×, corresponding to a pixel size of 0.859 Å. The defocus range was set from –1.0 to –2.0 μm. These movie frames were recorded without gain normalization and with TIFF-LZW compression. The data collection was performed in counting mode, with a total dose of ~80 electrons $Å^{-2}$ and a total exposure of 3 s fractionated into 40 frames. A total of 19,635 videos were recorded.

Single Particle Image Analysis

Single particle image analysis was performed using CryoSPARC ver. 4.6.2. After patch motion correction was performed to align all micrographs and estimate the contrast transfer function (CTF) parameters, particles representing proteins were automatically chosen by auto-picking, and the selected particles were extracted into a box of 256 × 256 pixels. A total of 894,325 particles were selected from the 10,399,280 auto-picked particles using 2D classification and binning by 4. Subsequently, the selected particles were re-extracted from the unbinned images into 320 × 320 pixels after reference-based motion correction. The initial 3D reference was obtained using ab-initio reconstruction. Heterogeneous refinement into three classes with C1 symmetry yielded a single clear class (466,989 particles). The 3D classification into three classes with C1 symmetry revealed two clear classes (144,996 and 153,849 particles, referred to as forms 1 and 2, respectively). Heterogeneous refinement into three classes with C1 symmetry was conducted for sADH forms 1 and 2, and each showed a single clear class (111,819 and 119,667 particles). Final density maps with 2.71 and 2.69 Å resolution were obtained after Fourier shell correlation (FSC)-mask auto-tightening and subsequent CTF refinement. The entire process is summarized in Fig. S3. The numerical data are listed in Table S2.

Molecular Modeling

Atomic models of sADH forms 1 and 2 were built using the Crystallographic Object-Oriented Toolkit (COOT). PHENIX was used for real-space refinement of the models based on maps of sADH forms 1 and 2

obtained using cryo-EM. The cofactors were added according to previously described methods. The atomic models of form 1 included residues 35−757 in the L subunit (723 residues); 42−76, 81–110, 117–147, and 166–455 in the C subunit (386 residues); and 27−131 in the S subunit (105 residues). The atomic models of form 2 included residues 35−757 in the L subunit (723 residues); 51–61, 117–136, and 174–455 in the C subunit (313 residues); and 27−131 in the S subunit (105 residues). The cryo-EM density maps were deposited in the Electron Microscopy Data Bank with the accession codes EMD-66439 (form 1) and 66440 (form 2). Atomic coordinates were deposited in the Protein Data Bank with accession codes 9X0Q (form 1) and 9X0R (form 2).

Molecular Dynamics Simulation

System Preparation

An enzyme–lipid complex was constructed using the Membrane Builder module of CHARMM-GUI [7]. The structure of ADH was obtained from the Protein Data Bank (PDB: 8GY2). Prior to system construction, all the cofactors present in the PDB structure were removed to simplify the model. The lipid bilayer was generated with a composition of phosphatidylcholine:phosphatidylethanolamine:phosphatidylglycerol:cardiolipin = 51.5:21.7:19.8:7.0, according to the literature data for components of the inner membrane of *Gluconobacter* sp. [8]. The initial orientation of ADH was manually adjusted such that the C subunit was partially embedded within the lipid bilayer. The system was solvated with TIP3P water molecules, and KCl was added at a final concentration of 150 mM.

Gaussian Accelerated Molecular Dynamics (GaMD)

The dual-boost GaMD simulation was performed using NAMD 3.0 and the CHARMM36 force field. Before the GaMD runs, a short conventional MD (cMD) phase of 2 ns was used for system equilibration. The GaMD boost parameters (threshold energy (E) and harmonic force constant (k)) were automatically calculated according to a standard protocol [9]. After equilibration, the GaMD production simulations were run for 300 ns

at 303.15 K and 1 atm. Bonds containing hydrogen atoms were restrained using the SHAKE algorithm [10] with a time step of 2 fs. Structural and dynamic properties were calculated from the trajectories using VMD.

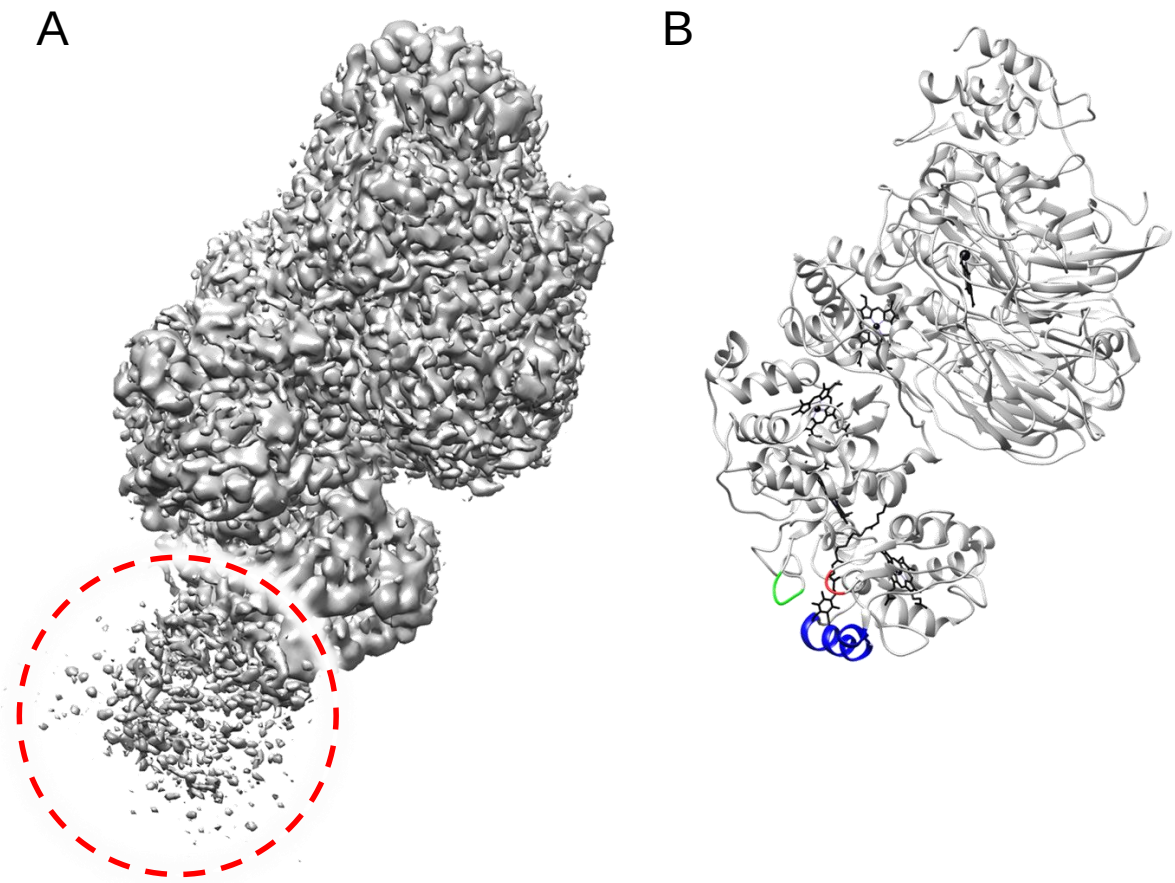

Fig. S1. (A) Cryo-EM map of ADH (EMDB: EMD-34368). (B) Corresponding cartoon structure of ADH (PDB: 8GY2). Dotted circle indicates noise of map derived from surfactants. Regions 1, 2, and 3 are highlighted in red, blue, and green, respectively.

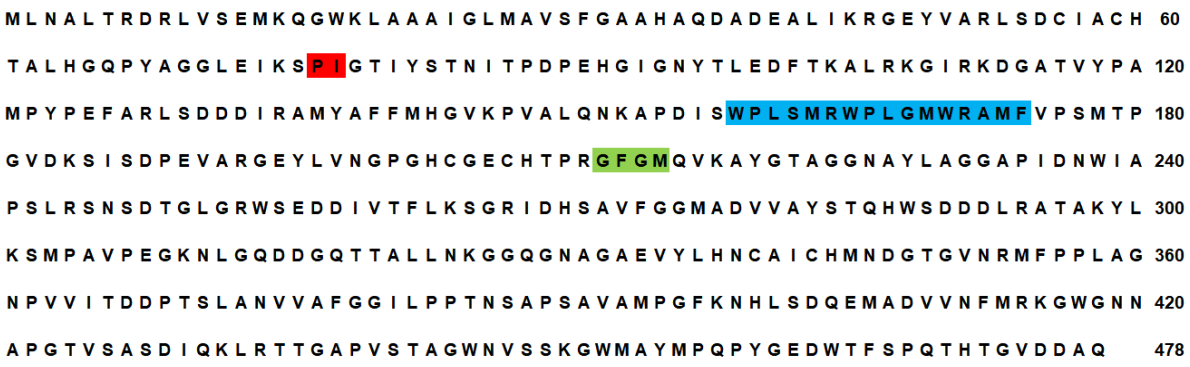

Fig. S2. Amino acid sequence of the C subunit of ADH. Regions 1, 2, and 3 are highlighted in red, blue, and green, respectively.

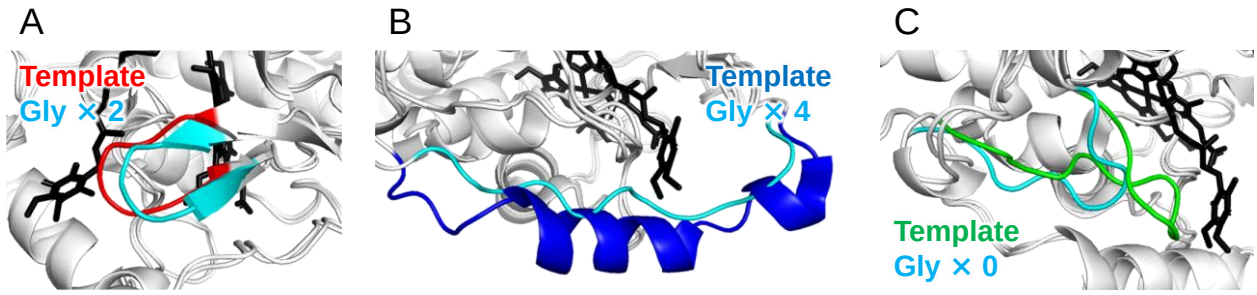

Fig. S3. Comparison of regions 1 (A), 2 (B), and 3 (C) between template structures from ADH and predicted structures created by AlphaFold3.

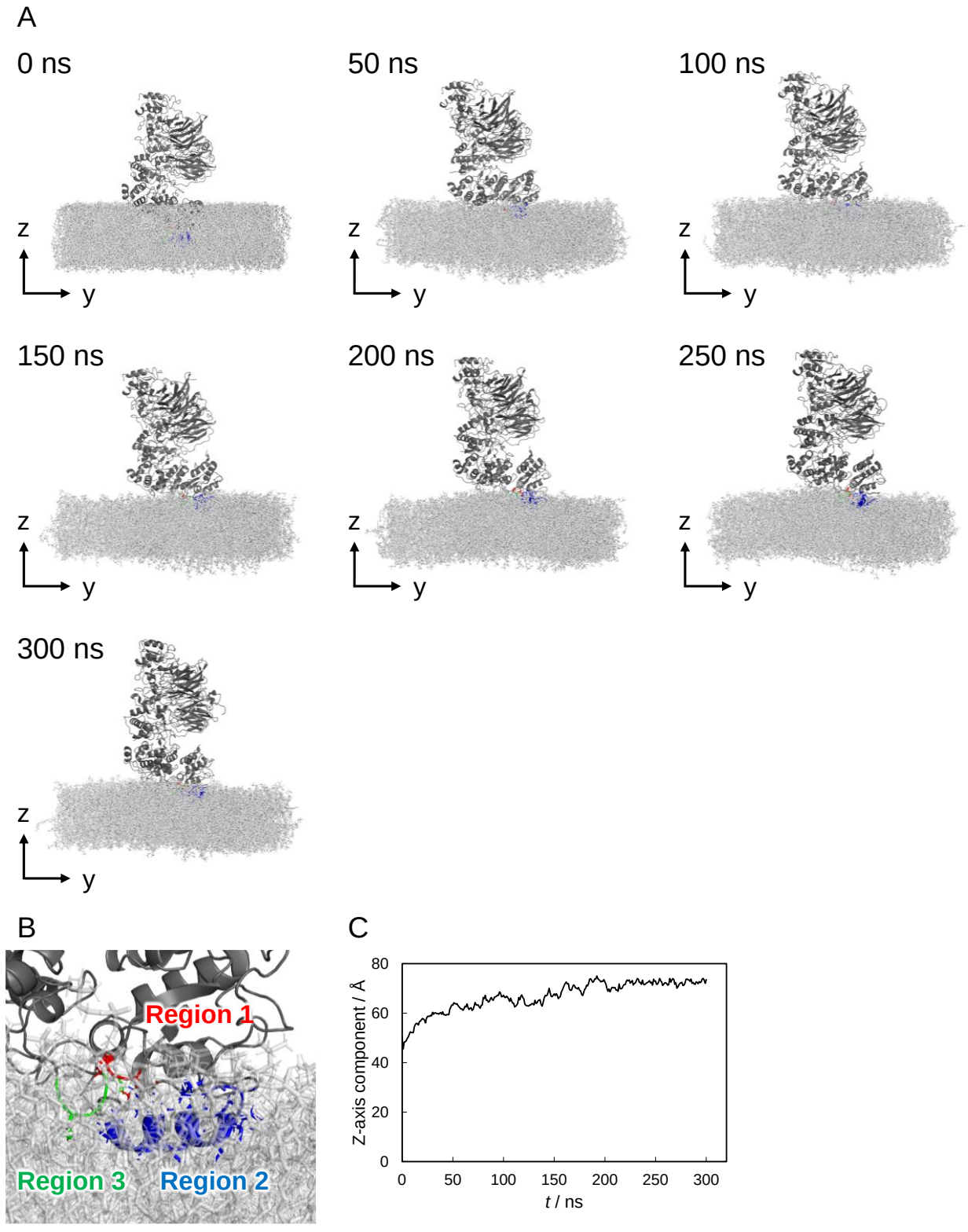

Fig. S4. (A) Structural snapshots of MD simulations of ADH-lipid complex (every 50 ns). Dark gray: ADH. Light gray: lipid. Red: region 1. Blue; region 2. Green: region 3. (B) Enlarged view of predicted membrane-binding regions at 300 ns. (C) Time-dependent transition in the Z-axis component of ADH.

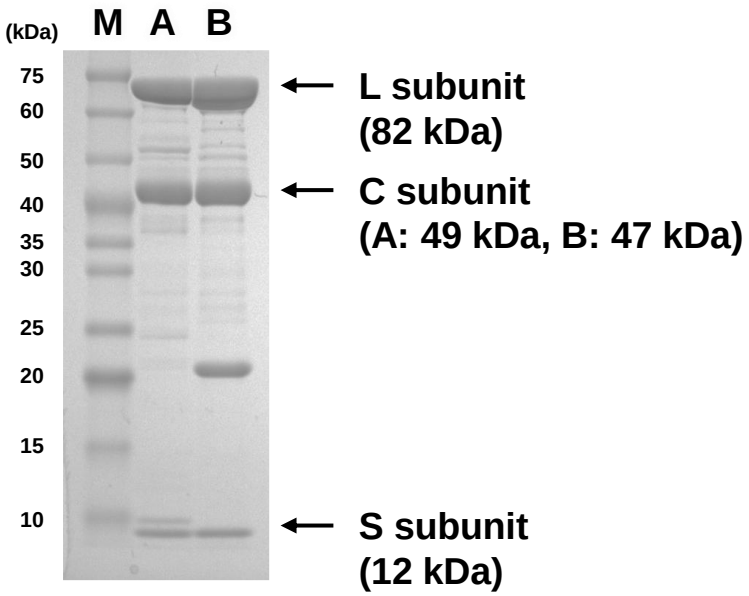

Fig. S5. SDS-PAGE analysis of rADH (A) and sADH (B). Lane M is the standard protein. Numbers written on the left side of the bands indicate the approximate molecular mass in units of kDa.

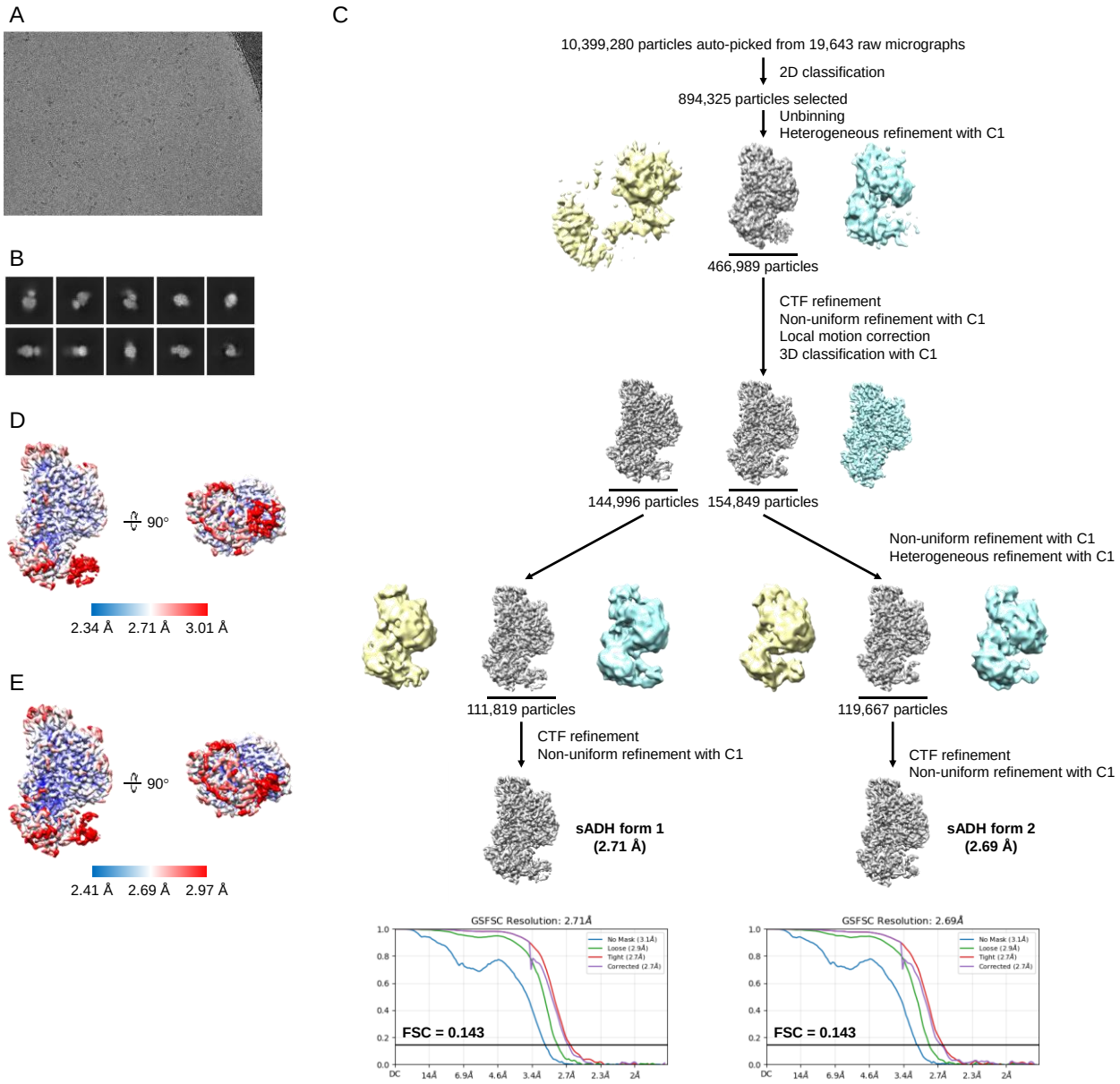

Fig. S6. Cryo-EM analysis of sADH. (A) Representative cryo-EM image of the data collection. (B) Various view of 2D class averages. (C) Flowchart of the cryo-EM single particle image analysis and FSC curves of the final density maps. (D) Local resolution of the final density map of sADH form 1 colored from blue (2.34 Å) to red (3.01 Å). (E) Local resolution of the final density map of sADH form 2 colored from blue (2.41 Å) to red (2.97 Å).

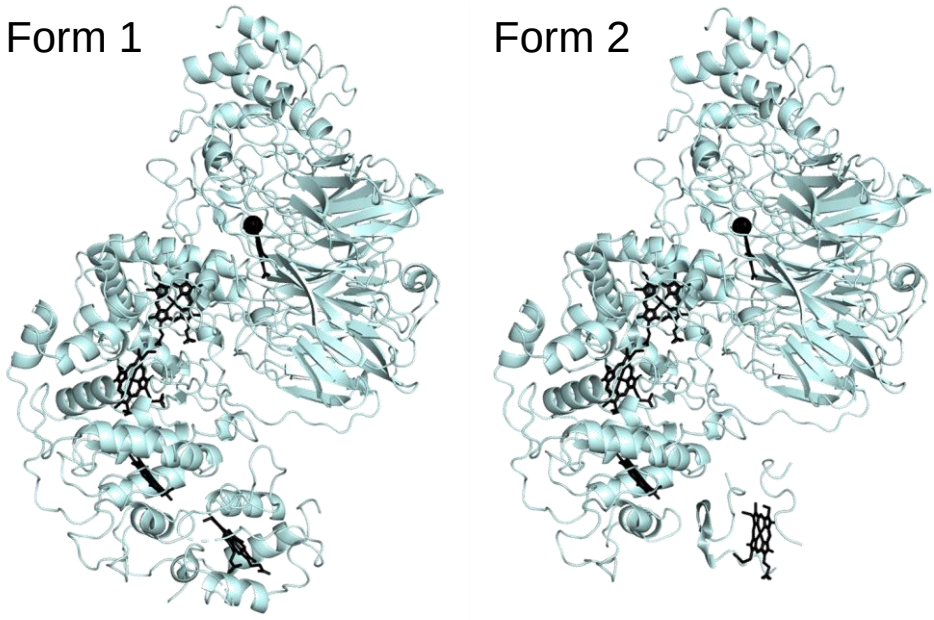

Fig. S7. 3D structure of sADH (form 1, PDB: 9X0Q) and sADH (form 2, PDB: 9X0R).

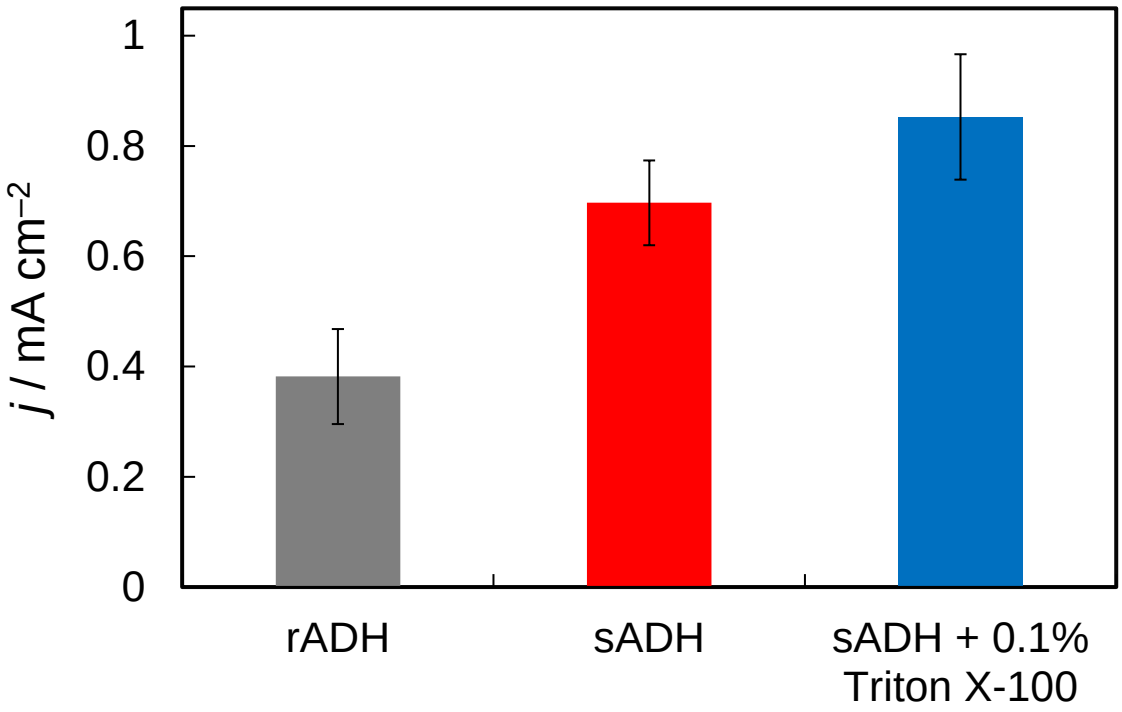

Fig. S8. Current density at rADH/CNT-COOH/GCE (black), sADH/CNT-COOH/GCE (red), and sADH/CNT-COOH/GCE prepared with 0.1% Triton X-100 (blue) at E = 0.5 V. Errors were determined using the Student's t distribution at 90% confidence level (n = 6).

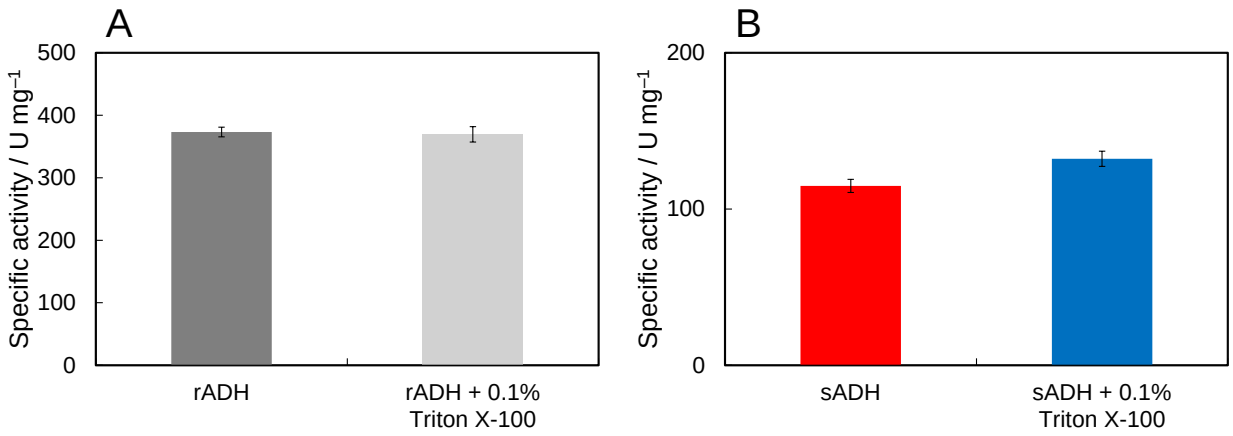

Fig. S9. Specific activity of rADH (A) and sADH (B) in solution in the absence and presence of 0.1% Triton X-100. Errors were determined using the Student's *t* distribution at 90% confidence level ($n = 6$).

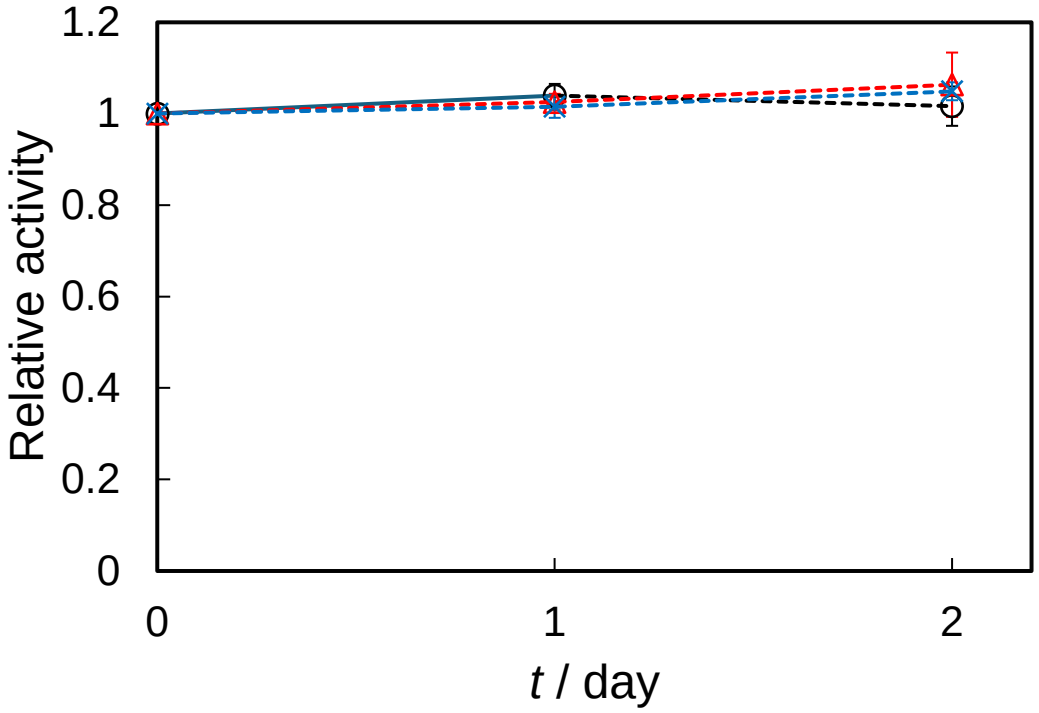

Fig. S10. Stability of the relative activity for ferricyanide reduction of rADH (black circles), sADH stored without Triton X-100 (red triangles), and sADH stored with 0.1% Triton X-100 (blue crosses). The enzymes were stored at 25 °C in 100 mM acetate buffer (pH 5.5) containing 10% sucrose. Errors were determined using the Student's *t* distribution at 90% confidence level ($n = 6$).

Table S1. Bacterial strains and plasmids used in this study.

Strain or plasmid	Description	Reference / Source
Strains		
Escherichia coli		
DH5α	F⁻ *endA1 hsdR17*(rk⁻ mk⁻) *supE44 thi-1* λ⁻ *recAl gyrA96 relA1 deoR* Δ(*lacZYA-argF*)U169 ϕ80d*lacZ*ΔM15	[11]
HB101	F⁻ *thi-1 hsdS20*(rB mB) *supE44 recA13 ara14 leuB6 proA2 lacY1 galK2 rpsL20* (Strr *xyl-5 mtl-1* λ⁻)	[12]
Gluconobacter oxydans		
Δ*adhAB* Δ*aldFGH* variant	NBRC12528 Δ*adhAB* Δ*aldFGH*	[1]
rADH expression vector	NBRC12528 Δ*adhAB* Δ*aldFGH* pBBR1MCS-4-Padh-*adhSAB*:: Ap^r	This study
Δ1 variant expression vector	NBRC12528 Δ*adhAB* Δ*aldFGH* pBBR1MCS-4-Padh-Δ1 variant:: Ap^r	This study
Δ2 variant expression vector	NBRC12528 Δ*adhAB* Δ*aldFGH* pBBR1MCS-4-Padh-Δ2 variant:: Ap^r	This study
Δ3 variant expression vector	NBRC12528 Δ*adhAB* Δ*aldFGH* pBBR1MCS-4-Padh-Δ3 variant:: Ap^r	This study
Δ1Δ2 variant expression vector	NBRC12528 Δ*adhAB* Δ*aldFGH* pBBR1MCS-4-Padh-Δ1Δ2 variant:: Ap^r	This study
Δ1Δ3 variant expression vector	NBRC12528 Δ*adhAB* Δ*aldFGH* pBBR1MCS-4-Padh-Δ1Δ3 variant:: Ap^r	This study
Δ2Δ3 variant expression vector	NBRC12528 Δ*adhAB* Δ*aldFGH* pBBR1MCS-4-Padh-Δ2Δ3 variant:: Ap^r	This study
Δ1Δ2Δ3 variant expression vector	NBRC12528 Δ*adhAB* Δ*aldFGH* pBBR1MCS-4-Padh-Δ1Δ2Δ3 variant:: Ap^r	This study
Plasmids		
pKR2013	Plasmid that mediates plasmid transfer; Km^r	[13]
pBBR1MCS-4	Broad-host-range plasmid; *mob* Ap^r	[14]
pBBR1MCS-4-Padh	pBBR1MCS-4, a 0.7-kb fragment of a promoter region of the *adhAB* genes of *G. oxydans* 621H	[15]
pBBR1MCS-4-Padh-rADH	pBBR1MCS-4-Padh, a 4.2-kb fragment of the *adhSAB* genes of *G. oxydans* NBRC12528 shortening non-coding sequences	This study
pBBR1MCS-4-Padh-Δ1 variant	pBBR1MCS-4-Padh-rADH, deleting a sequence corresponding to region 1 and inserting a sequence corresponding to a di-glycine linker	This study
pBBR1MCS-4-Padh-Δ2 variant	pBBR1MCS-4-Padh-rADH, deleting a sequence corresponding to region 2 and inserting a sequence corresponding to a tetra-glycine linker	This study
pBBR1MCS-4-Padh-Δ3 variant	pBBR1MCS-4-Padh-rADH, deleting a sequence corresponding to region 3	This study
pBBR1MCS-4-Padh-Δ1Δ2 variant	pBBR1MCS-4-Padh-rADH, deleting two	This study

	sequences corresponding to regions 1 and 2, respectively, and inserting two sequences corresponding to di-glycine and tetra-glycine linkers, respectively	
pBBR1MCS-4-Padh-Δ1Δ3 variant	pBBR1MCS-4-Padh-rADH, deleting two sequences corresponding to regions 1 and 3, respectively, and inserting a sequence corresponding to a di-glycine linker	This study
pBBR1MCS-4-Padh-Δ2Δ3 variant	pBBR1MCS-4-Padh-rADH, deleting two sequences corresponding to regions 2 and 3, respectively, and inserting a sequence corresponding to a tetra-glycine linker	This study
pBBR1MCS-4-Padh-Δ1Δ2Δ3 variant	pBBR1MCS-4-Padh-rADH, deleting three sequences corresponding to regions 1, 2, and 3, respectively, and inserting two sequences corresponding to di-glycine and tetra-glycine linkers, respectively	This study

Table S2. EM data collection, processing, and refinement statistics.

		sADH (form 1) (EMD-66439, PDB: 9X0Q)	sADH (form 2) (EMD-66440, PDB: 9X0R)
Data collection and processing	Magnification	60,000	60,000
	Voltage (kV)	300	300
	Electron exposure (e^{-}/Å^{-2})	80	80
	Defocus range (μm)	−1.0 – −2.0	−1.0 – −2.0
	Pixel size (Å)	0.859	0.859
	Symmetry imposed	C1	C1
	Initial particle images (no.)	10,399,380	10,399,380
	Final particle images (no.)	111,819	119,667
	Map resolution (Å)	2.7	2.7
	FSC threshold	0.143	0.143
	Map resolution range	2.34–3.08	2.41–3.00
Refinement	Initial model used	De novo	De novo
	Model resolution	2.7	2.7
	FSC threshold	0.143	0.143
	Model resolution range	80-2.7	80-2.7
	Map sharpening *B* factor (Å^2)	–90.2	–92.0
	Model composition		
	Non-hydrogen atoms	9535	8,969
	Protein residues	1216	1143
	Ligands	6	6
	B factors (Å^2)		
	Protein	49.23	81.65
	Ligand	49.24	88.39
	R.M.S.D		
	Bond length (Å)	0.003	0.002
	Bond angles (°)	0.588	0.546
	Validation		
	MolProbity score	2.02	2.17
	Clash score	7.38	8.55
	Poor rotamers (%)	2.07	2.64
	Ramachandran plot		
	Favored (%)	94.52	94.26
	Allowed (%)	5.48	5.74
	Disallowed (%)	0	0

References

[1] K. Ichikawa, T. Adachi, Y. Kitazumi, O. Shirai, K. Sowa, *ACS Catal.*, 2025, **15**, 7283–7295.

[2] T. Adachi, K. Sowa, Y. Kitazumi, O. Shirai, K. Kano, *Bioelectrochemistry*, 2022, **143**, 107992.

[3] M. Ameyama, E. Shinagawa, K. Matsushita, O. Adachi, *J. Bacteriol*., 1981, **145**, 814–823.

[4] B. Carragher, Y. Cheng, A. Frost, R. M. Glaeser, G. C. Lander, E. Nogales, H.-W. Wang, *J. Microsc.*, 2019, **276**, 39–45.

[5] D. N. Mastronarde, *J. Struct. Biol.*, 2005, **152**, 36–51.

[6] K. Yonekura, S. Maki-Yonekura, H. Naitow, T. Hamaguchi, K. Takaba, *Commun. Biol.*, 2021, **4**, 1044.

[7] E. L. Wu, X. Cheng, S. Jo, H. Rui, K. C. Song, E. M. Dávila-Contreras, Y. Qi, J. Lee, V. Monje-Galvan, R. M. Venable, J. B. Klauda, W. Im, *J. Comput. Chem.*, 2014, **35**, 1997–2004.

[8] Y. Tahara, Y. Yamada, K. Kondo, *Agric. Biol. Chem.*, 1976, **40**, 2355–2360.

[9] Y. T. Pang, Y. Miao, Y. Wang, J. A. McCammon, *J. Chem. Theory Comput.*, 2017, **13**, 9–19.

[10] J. P. Ryckaert, G. Ciccotti, H. J. C. Berendsen, *J. Comput. Phys.*, 1977, **23**, 327–341.

[11] S. G. Grant, J. Jessee, F. R. Bloom, D. Hanahan, *Proc. Natl. Acad. Sci. U. S. A.*, 1990, **87**, 4645–4649.

[12] H. W. Boyer, D. Roulland-Dussoix, *J. Mol. Biol.*, 1969, **41**, 459–472.

[13] D. H. Figurski, D. R. Helinski, *Proc. Natl. Acad. Sci. U. S. A.*, 1979, **76**, 1648–1652.

[14] M. E. Kovach, P. H. Elzer, D. S. Hill, G. T. Robertson, M. A. Farris, R. M. Roop II, K. M. Peterson, *Gene*, 1995, **166**, 175–176.

[15] S. Kawai, M. Goda-Tsutsumi, T. Yakushi, K. Kano, K. Matsushita, *Appl. Environ. Microbiol.*, 2013, **79**, 1654–1660.